

Progress in Space Flight Environment Effects: Predicting Spacecraft Single Event Environments with the FLUKA Monte Carlo Nuclear Reaction and Transport Code

Steven L. Koontz, *Johnson Space Center*
Brandon D. Reddell, *Johnson Space Center*

Paul Boeder, *The Boeing Company*

Abstract

The contribution of nuclear reactions and secondary particle showers, caused by cosmic ray interactions with spacecraft materials, to spacecraft avionics system single event environments is explored using the FLUKA Monte Carlo nuclear reaction and transport code and spacecraft in-flight single event upset (SEU) data.

Introduction

Natural space flight ionizing radiation (IR) environments are radically different from the IR environments, both natural and artificial, encountered on Earth's surface. The space flight IR environment is dominated by high-kinetic-energy-charged particles with relatively small contributions from x-rays and gamma rays, and essentially no contribution from the natural radioisotope decay processes that dominate the natural Earth surface IR environment. The energetic charged particles of interest consist of galactic and solar cosmic rays and energetic charge particles trapped in planetary magnetospheres (e.g., Earth's Van Allen belts), and can interact with spacecraft materials to produce both ionization along the particle track through the material and secondary particle showers following collisions with spacecraft nuclei. Energetic charged particles are the ultimate cause of spacecraft SEUs (i.e., effects caused by a single energetic charged particle), and they determine the character of the spacecraft avionics single event effect (SEE) environment and, ultimately, spacecraft safety and reliability.

Preliminary results of FLUKA Monte Carlo nuclear reaction and transport code calculations of spacecraft SEE environments and the corresponding electronic device event rates are reported in this paper.

First, **FLUKA** (i.e., **FLUK**tuierende **K**askade)-based calculations of spacecraft avionics SEE and corresponding SEU rates are compared with in-flight data for several spacecraft avionics devices as a first step in evaluating the FLUKA code for spacecraft SEE applications.

Second, CRÈME-96 deterministic modeling of SEU rates and Petersen Figure of Merit (FOM) are also compared to FLUKA SEU rate estimates and in-flight data, to further validate the FLUKA-based methods against widely used

semi-empirical methods for those cases in which all three methods are applicable.

Finally, the effects, on device SEE rates, of incorporating thin (1 micron) heavy element metallization layers into microelectronic circuits are examined using the FLUKA-based methods reported here.

Results/Discussion

Table 1 and figure 1 compare in-flight SEU rates for various complementary metal oxide semiconductor (CMOS) spacecraft micro-devices with estimates produced using the FLUKA code applied to a generic three-dimensional "spacecraft" consisting of concentric spherical shells of spacecraft shielding mass material with thin (10 micron) silicon detector shells placed at various shielding mass depths. Thin layers (1 micron) of high atomic number elements such as silver (Ag), Hafnium (Hf), tungsten (W), or lead (Pb) can be placed on the silicon detector shells. On-orbit SEU rate estimates produced with the FOM and the two-dimensional deterministic CRÈME-96 codes are shown in figure 1 and Table 1 for purposes of comparison. Rates are compared at the same estimated median spacecraft shielding mass as well as the same device cross section and device thickness parameters.

As can be seen in figure 1, the three SEU rate estimation methods provide comparable accuracy, are generally within a factor of 10 of the on-orbit rate, and often much better—an accuracy that is more than adequate for practical avionics systems design and verification purposes. The three SEU rate estimators are compared using the least squares performance metric that measures the net deviation of the various SEU rate estimates with observed in-flight SEU rates.

It is interesting to note that the accuracy of FLUKA predictions of Mercury Messenger static random access memory (SRAM) SEU rates improves dramatically when a 1-micron W film is placed in contact with the outer surface of each silicon detector shell—an expected outcome given the probable role of W in Mercury Messenger SRAM SEU sensitivity. FLUKA simulations show that the magnitude of the W film effect increases the SEU rate at higher shielding mass by as much as three orders of magnitude for high

Progress in Space Flight Environment Effects: Predicting Spacecraft Single Event Environments with the FLUKA Monte Carlo Nuclear Reaction and Transport Code

continued

linear energy transfer (LET) threshold (> 4 megaelectron volt centimeter squared per milligram [$\text{MeV cm}^2/\text{mg}$]) devices but was unobservable for low LET threshold devices (< 4 [$\text{MeV cm}^2/\text{mg}$]).

Figures 2 and 3 show the results of FLUKA-based calculations demonstrating the effects of thin W layers proximal to the silicon scoring detector shells in the concentric spherical shell “spacecraft” model used in the FLUKA simulations. The 1977 solar minimum interplanetary galactic cosmic ray spectrum is the natural space radiation environment and the spacecraft shielding mass is aluminum (Al) in the subject calculations. In both figures, the total flux of charged particles with LET values greater than some threshold value X is plotted as a function of Al shielding mass for the corresponding silicon detector shell. The values of X are, in order from maximum to minimum particle flux, 0.001, 0.012, 0.120, 1.30, 4.03, 9.8, 15, and 30 $\text{MeV cm}^2/\text{mg}$. The model used to generate the figure 2 data contained only 10 micron silicon detector shells while for the figure 3 data, 1 micron of W was placed in contact with the outer surface of each silicon detector shell. Two statistically independent FLUKA Monte Carlo runs were averaged to produce the data in figures 2 and 3.

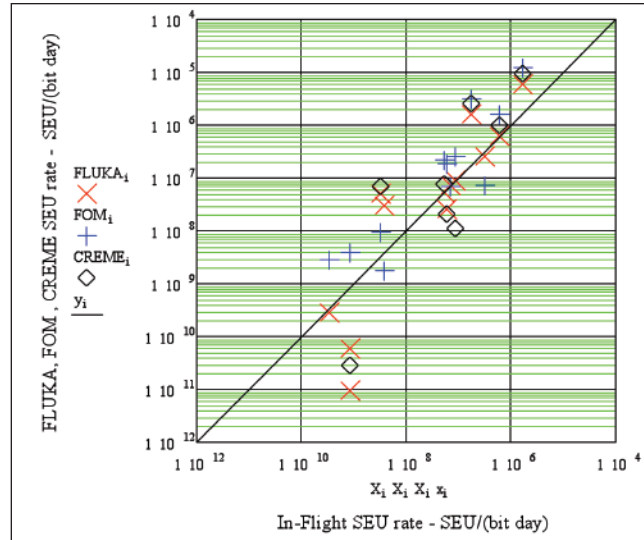


Fig. 1. In-flight single event upset (SEU) rates vs. predicted SEU rates.

Comparison of the two figures shows no remarkable differences until the magnitude of particle LET is greater than 4 ($\text{MeV cm}^2/\text{mg}$). As expected, both figures show a rapid increase in the total particle flux above threshold as the LET threshold is increased from 0.001 $\text{MeV cm}^2/\text{mg}$ to 30 $\text{MeV cm}^2/\text{mg}$. However, substantial differences in the total particle flux are apparent for LET threshold values of 9.8, 15, and 30 $\text{MeV cm}^2/\text{mg}$, especially at higher shielding mass values, with the W case showing much higher fluxes than the no-W case. The flux of particles with $\text{LET} > 30$ $\text{MeV cm}^2/\text{mg}$ is zero at all shielding masses for the no-W case, while in the W case the $\text{LET} > 30$ $\text{MeV cm}^2/\text{mg}$ flux is between 0.1 and 1.0 per day at nearly all shielding masses. The relatively high flux of particles with $\text{LET} > 10$ $\text{MeV cm}^2/\text{mg}$ in the W case implies an increased risk of both hard (destructive) and soft (recoverable) avionics

Table 1. Predicted vs. Observed In-flight Single Event Upset Rates for Complementary Metal Oxide Semiconductor Micro-Devices (International Space Station [ISS], Interplanetary [IP], Geosynchronous [GEO] spacecraft flight data).

Spacecraft Identifier	Flight Environment	Device Part Number or other identifier	Median Shielding Mass g/cm^2	In-Flight SEU/bit day (X)	FLUKA Predicted SEU/bit day (FLUKA)	CRÈME-96 Predicted SEU/bit day (CRÈME)	Petersen Figure of Merit (FOM) Predicted SEU/bit day (FOM)
ISS	ISS	TMS44400	10	8.5×10^{-8}	8.9×10^{-8}	1.1×10^{-7}	2.5×10^{-7}
ISS	ISS	TMS44400	40	7.0×10^{-8}	7.2×10^{-8}	3.1×10^{-8}	6.8×10^{-8}
ISS	ISS	SMK416400	10	3.2×10^{-9}	5.1×10^{-8}	7.2×10^{-8}	9.6×10^{-9}
ISS	ISS	SMK416400	40	3.7×10^{-9}	2.8×10^{-8}	2.0×10^{-8}	2.1×10^{-9}
ISS	ISS	KM44S32030T-GL	40	3.3×10^{-10}	2.2×10^{-10}	1.9×10^{-10}	2.0×10^{-10}
Space Shuttle	ISS	IMS1601EPI	34	3.1×10^{-7}	2.5×10^{-7}	2.7×10^{-7}	7.4×10^{-8}
Thuraya	GEO	ASIC 0.25 μ static random access memory, IBM SA-12	0.7	5.3×10^{-8}	5.3×10^{-8}	7.9×10^{-8}	2.2×10^{-7}
Mercury Messenger	IP	ASIC “rad/single event effect hard” static random access memory	1.0	8.6×10^{-10}	5.8×10^{-11} (W)	2.9×10^{-11}	4.0×10^{-9}
Mercury Messenger	IP	ASIC “rad/single event effect hard” static random access memory	1.0	8.6×10^{-10}	9.3×10^{-12} (no-W)	2.9×10^{-11}	4.0×10^{-9}
Cassini	IP	OKI (4Mx1)	3.4	5.8×10^{-8}	2.5×10^{-8}	2.1×10^{-8}	1.9×10^{-7}
Solar Heliospheric Observatory	IP	SMJ44100	1.0	5.9×10^{-7}	6.4×10^{-7}	1.2×10^{-6}	1.6×10^{-6}
Solar Heliospheric Observatory	IP	CP65656EV	1.0	1.7×10^{-7}	1.6×10^{-6}	2.5×10^{-6}	3.1×10^{-6}
ETS-V (Engineering Test Satellite V)	GEO	PD4464D-20	5.8	1.7×10^{-6}	6×10^{-6}	9.3×10^{-6}	1.2×10^{-5}

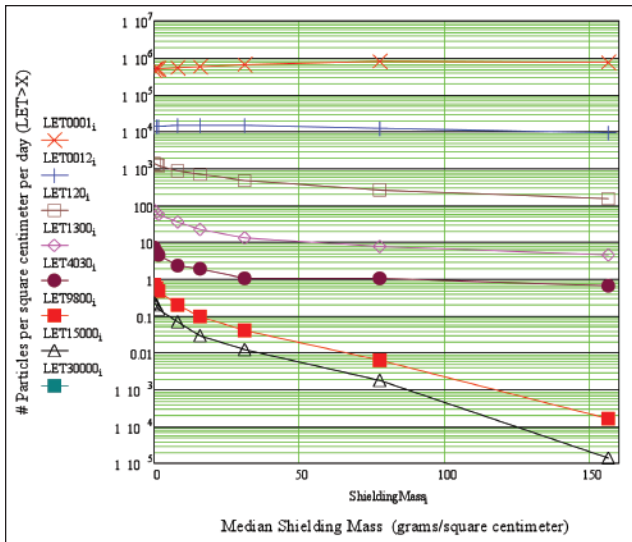


Fig. 2. Particle flux vs. shielding mass – no tungsten.

SEE effects, even at high shielding mass, that would not be anticipated on the basis of experience with silicon-based microelectronic devices that do not contain W. The increasing use of high atomic number (Z) elements in modern electronic devices presents new avionics risk factor that must be addressed with innovative spacecraft avionics design, test, and verification techniques.

The fissility factor is a metric describing the relative likelihood of an energetically excited nucleus to decay by fission as opposed to other decay modes. If 1-micron films of elements other than W are placed in contact with the silicon detector shells, the relative flux of particles with $LET > 10 \text{ MeV cm}^2/\text{mg}$ into the silicon detector should increase with the fissility factor (Z^2/A) of the elements, at least for $Z > 40$. Figure 4 shows the fissility parameter correlation with the $X > 10 \text{ MeV cm}^2/\text{mg}$ particle flux (normalized with respect to W) entering the silicon detector shells at median shielding masses of 31 (\square) and 77 (\diamond) grams per centimeter squared (g/cm^2) Al with the 1-micron over-layers of the elements shown in Table 2. When measured fission probabilities are plotted against the fissility parameter, the curve displays a minimum around atomic number 40 and increases rapidly as atomic number increases above 40 and decreases below 40. The fissility parameter itself only describes the relative likelihood of fission, not the LET range of the fission products. The number of high LET fragments produced by a fission event will depend on the atomic number of the parent nucleus. Low-Z nuclei simply can't produce the high-Z, high-LET fragments that high-Z nuclei can produce. Relative fission probabilities (\circ , also normalized with respect to W) are also plotted in figure 4 for comparison. The trend in fission probability is in reasonable agreement with the FLUKA calculations of $LET > 10 \text{ MeV cm}^2/\text{mg}$ particle flux into the silicon detector shells.

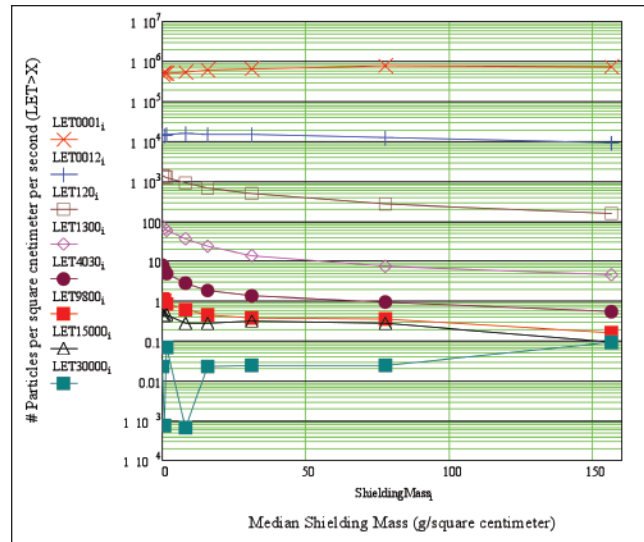


Fig. 3. Particle flux vs. shielding mass – tungsten.

Table 2. Silicon Detector Shell Over-Layer Elements and Fissility Parameters for Figure 4

Element	Aluminum (Al)	Silver (Ag)	Hafnium (Hf)	Tungsten (W)	Lead (Pb)
Fissility Factor	6.259	20.434	29.124	29.923	30.918

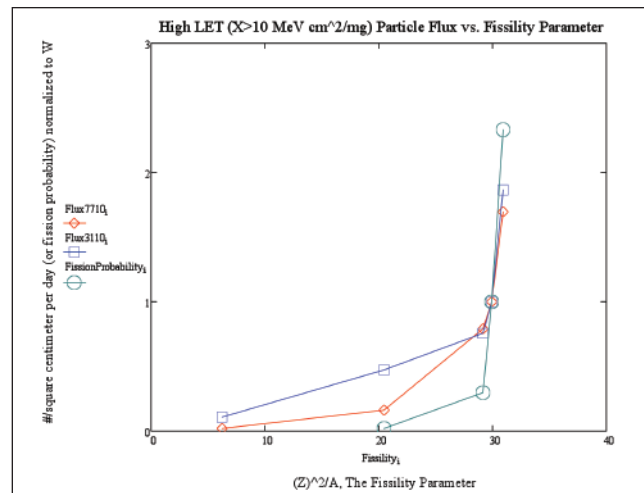


Fig. 4. One micron over-layers on silicon detector shells.

Conclusions

FLUKA can be used to calculate estimates of spacecraft SEE environments and the corresponding microelectronic device SEE upset rates. In comparable cases, FLUKA-based calculations compare favorably with CRÈME-96 and FOM estimates of in-flight SEE rates.

Finally, the FLUKA based SEU rate estimation method outlined here has been shown to be useful in evaluating the effect of incorporating heavy elements into microelectronic devices on device SEE rates—evaluations that cannot be performed with CRÈME-96 or FOM. FLUKA-based methods also enable investigations of the effects of spacecraft microelectronic elemental composition as well as spacecraft shielding mass elemental composition; i.e., cases in which CRÈME-96 and the FOM are not applicable.